SCIPEDIA

A Solar Irradiance Prediction Model with Recurrent Neural Networks and Computer Graphics Methods

Woosuk Shin[1] and Nakhoon Baek[1,2,3,*]

[1] School of Computer Science and Engineering, Kyungpook National University, Daegu, 41566, Republic of Korea

[2] Graduate School of Data Science, Kyungpook National University, Daegu, 41566, Republic of Korea

[3] Data-Driven Intelligent Mobility ICT Research Center, Kyungpook National University, Daegu, 41566, Republic of Korea

INFORMATION

Keywords:
Recurrent neural networks
3D environmental simulation
solar irradiance prediction
astronomical factors
atmospheric factors

DOI: 10.23967/j.rimni.2025.10.58701

SCIPEDIA Revista Internacional de Métodos Numéricos para Cálculo y Diseño en Ingeniería

Revista Internacional Métodos numéricos para cálculo y diseño en ingeniería RIMNI CIMNE

A Solar Irradiance Prediction Model with Recurrent Neural Networks and Computer Graphics Methods

Woosuk Shin[1] **and Nakhoon Baek**[1,2,3,*]

[1]School of Computer Science and Engineering, Kyungpook National University, Daegu, 41566, Republic of Korea

[2]Graduate School of Data Science, Kyungpook National University, Daegu, 41566, Republic of Korea

[3]Data-Driven Intelligent Mobility ICT Research Center, Kyungpook National University, Daegu, 41566, Republic of Korea

ABSTRACT

This paper presents a computer simulation model for predicting solar irradiance in a three-dimensional (3D) environment. Solar irradiance prediction is critical for solar energy systems and related fields. Machine learning techniques, such as recurrent neural networks (RNNs), are employed for more accurate predictions. Integrating a 3D environmental simulation with the RNN models achieves accurate predictions with reasonable resolutions. The training model uses selected astronomical and atmospheric factors to train the RNN models. The proposed method allows the user to obtain the corresponding solar irradiance prediction values for arbitrary periods. Astronomical and atmospheric factors affect solar irradiance; hence, data from the Korea Meteorological Administration are used for training. The RNNs, including the long short-term memory (LSTM) and gated recurrent unit methods, are employed for the prediction. The LSTM layers outperformed other configurations, accurately predicting zero irradiation values. A set of solar irradiance models is presented using RNNs by configuring their layers, and the layout consisting of four LSTM layers performed best. This layout achieved reasonable error bounds, with relatively good root mean squared error and mean absolute error values. A computer graphics-based solar irradiance prediction model is proposed based on this prediction model, incorporating simulations of the surrounding environment. A case study is presented with surrounding buildings to analyze the solar irradiance over the year with a one-hour forecasting horizon to demonstrate its feasibility. Moreover, we plan to improve the results with other neural network models, such as the fuzzy-embedded RNN.

OPEN ACCESS

Received: 19/09/2024

Accepted: 13/12/2024

DOI
10.23967/j.rimni.2025.10.58701

Keywords:
Recurrent neural networks
3D environmental simulation
solar irradiance prediction
astronomical factors
atmospheric factors

*Correspondence: Nakhoon Baek (nbaek@knu.ac.kr).

1 Introduction

1.1 Solar Irradiance Prediction

Solar irradiance prediction plays a critical role in analyzing the potential and performance of solar energy systems, guiding the design, operation, and planning of photo-voltaic installations [1–3]. Solar irradiance prediction involves computational modeling and analysis of the interactions between sunlight and the Earth's atmosphere concerning factors affecting the amount of solar radiation reaching the Earth's surface. Accurately predicting solar irradiance is essential to optimizing energy output, evaluating system efficiency, and ensuring the economic viability of solar projects [4,5]. Additionally, solar irradiance simulation aids in weather forecasting, climate studies, and research on solar resource availability [6,7].

1.2 Machine Learning Techniques

Recently, *machine learning* techniques have emerged as powerful tools. Among these tools, *deep neural networks* (DNNs) and *recurrent neural networks* (RNNs) have demonstrated tremendous potential due to their ability to capture and model the complex temporal dependencies in solar irradiance data [8,9]. While DNNs can also be employed to address forecasting problems, RNNs can manage nonlinear relationships and account for long-term data dependencies, which is critical to capturing the dynamics of solar irradiance accurately. Moreover, RNNs are also robust at handling different weather patterns and atmospheric influences because they can learn from historical data and adapt to changing environmental conditions [10–12].

Further, DNNs are widely applied in many *artificial intelligence* applications, including computer vision, speech recognition, image recognition, and robotics. Although DNNs deliver highly accurate prediction results on many tasks, they require high computational power due to their complexity. The higher complexity derives from multiple hidden layers. As DNNs are vulnerable to the overfitting problem [13], many studies have presented complicated methods to resolve them [14,15]. However, aside from the complexity, the DNN has demonstrated its strength in many areas due to its high accuracy and ability to adopt nonlinear combinations for input features [16,17].

Long short-term memory (LSTM) is a variant of the RNN designed to address the limitations in traditional RNNs [18]. These limitations are evident when predicting time-series data with long-term timestamps because they can cause problems, such as vanishing or exploding gradients, which result in incorrect predictions across the entire network. Consequently, LSTMs were introduced to address the challenge of long-term dependencies that traditional RNNs encounter. Furthermore, LSTM methods overcome this challenge by substantially modifying their recurrent layer by introducing a time-step cell unit, enabling information exchange between these layers. This innovation makes the LSTM network a widely adopted choice in contemporary applications involving sequential data prediction.

Gated recurrent unit (GRU) is another variation of RNNs, similar to LSTM. Compared to LSTM, GRU adopts much simpler cells, enabling a faster learning rate. However, it has lower accuracy than LSTM when training a large dataset.

1.3 Motivation

Although solar irradiance predictions using the stated machine learning techniques have been widely studied [19], other techniques also have important roles in prediction. In Ref. [20], the authors comprehensively researched solar irradiance forecasting models. These forecasting models are divided into *data-driven methods* and *image-based forecasting models*. Data-driven methods are divided into *time-series models*, *recursive least square models*, *machine learning*, and *sensor networks*. Satellite and

ground-based sky images can also be employed to predict solar irradiance by computing cloud motion vectors. The study found the best-performing forecasting methods for various forecast horizons, which are divided into *very short-term* (e.g., up to few minutes), *short-term* (e.g., 30 min to 6 h), *mid-term* (6 to 48 h), and *long-term* (3 to 10 day) horizons. According to the research, ground measurements perform best for very short-term horizons, whereas *cloud motion vectors* [21] perform better for short-term forecasts. For mid- and long-term forecasting, the *numerical weather prediction* model [22] performs best.

However, the authors aim to demonstrate that the numerical weather prediction model also performs well in short-term prediction. Therefore, the authors present a prediction model using machine learning techniques for numerical weather prediction. The presented model should predict solar irradiance with a 1-h forecast horizon, representing short-term prediction. Additionally, advances in computer graphics, ray tracing, and computational power have made it possible to simulate the solar irradiance distribution more accurately and efficiently, even in a 3D environment. These simulations reflect several factors, such as the Sun's position, terrain elevation, shading from buildings and vegetation, and atmospheric conditions. The 3D environmental simulations provide more realistic solar irradiance estimates by considering these variables, enabling improved energy planning, building design, and system performance evaluation.

Integrating solar irradiance prediction into a 3D environmental simulation offers several advantages. First, it allows the evaluation of *solar irradiance* in complex urban environments where shading and obstruction from buildings are significant factors. Second, it can evaluate the influence of architectural design and urban planning on solar power generation, promoting the development of energy-efficient buildings and sustainable urban environments. Additionally, *3D environmental simulations* can support decision-making processes by providing detailed insight into the expected solar irradiance patterns at various locations and times, aiding in selecting optimal sites for solar installations.

This paper presents *a computer simulation model* that can predict *solar irradiance* in situations where buildings, terrain, and natural objects are arranged. The algorithm consists of two principal steps. First, the solar irradiance at a specific location is predicted, assuming a flat plane with no surrounding obstacles. Public meteorological offices provide data on the solar irradiance at designated observatory locations, but there are no measured values at arbitrary locations. In addition, data for a period without observation data cannot be imported. Therefore, solar irradiance values for arbitrary locations and periods were predicted after training the artificial neural network models with previous solar irradiance data. This work contributes to determining the best performance model by examining tests with neural network models.

In the next step, a computer graphics simulation created shadows after arranging real or virtual buildings and obstacles around the desired location. Generating a shadow map for a specific period allows for accurate prediction of real-world solar irradiance. These models provide valuable insight into predicting solar irradiance accurately in a 3D or real-world environment, offering a new method for improved solar energy assessments, urban planning, and renewable energy integration.

Section 2 discusses the crucial astronomical and atmospheric features related to solar irradiance. The RNN models based on these features are presented in the next section. Computer graphics simulations and shadow map generations are explained in Section 5. The Section 6 presents a case study to demonstrate the feasibility of the proposed method. Finally, conclusions and future work are presented.

2 Feature Selection

Before presenting the overall methods, we present critical features related to solar irradiance. These features act as input or control parameters of the neural network model for predicting solar irradiance. *Astronomical factors*, including the geometric locations of the Earth and the Sun, primarily affect the amount of solar irradiance reaching the Earth's surface. The predominant astronomical factors directly related to solar irradiance are summarized below:

- **Solar Declination:** *Solar declination* represents the angle between the Sun's rays and the plane of the Earth's equator. This angle changes over the year due to the tilt of the Earth's axis. Thus, the Sun's position in the sky varies with the seasons. Higher solar declination during summer increases solar irradiance, whereas lower declination during winter decreases solar irradiance. The vernal and autumnal equinoxes at zero solar declination mark the transition between seasons.
- **Solar Zenith Angle:** The *solar zenith angle* is the angle between the Sun and a line perpendicular to the earth's surface. The angle depends on the observer's latitude, time of the day, and time of the year. A smaller solar zenith angle corresponds to a higher Sun position in the sky, resulting in more direct sunlight. In general, during the morning or evening hours or at high latitudes, larger solar zenith angles increase atmospheric attenuation and lower solar irradiance because sunlight travels a longer path through the atmosphere.
- **Earth-Sun Distance:** The distance between the Earth and Sun varies due to the elliptical shape of the Earth's orbit. Thus, the solar radiation the Earth receives varies throughout the year. Solar irradiance is slightly higher when the Earth is closer to the Sun (*perihelion*), typically in early January. Conversely, solar irradiance is slightly lower as the Earth moves away from the Sun (*aphelion*), typically at the beginning of July. Changes in distance affect the total solar irradiance received, but the effect is relatively negligible compared with other factors. This work applied the Earth-Sun distance from the *Landsat Missions* data provided by the *United States Geological Survey* [23]. Fig. 1 illustrates the changes in the Earth-Sun distance, in *astronomical units* by *day of the year*.

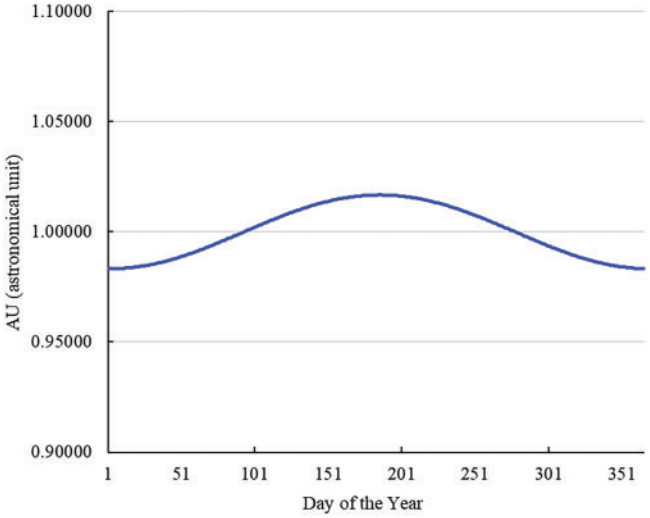

Figure 1: Earth-Sun distance in astronomical units by day of the year

The Earth orbits the Sun in a periodic orbit with slight fluctuations; hence, most previous work has focused on mathematically calculating the solar declination and solar zenith angle [24,25]. According to one study [26], both values can be calculated and converted into the relative position of the observed Sun at a particular location expressed with two angles: *solar altitude* and *solar azimuth*. For example, Fig. 2 depicts the calculated solar altitude and azimuth as a continuous line in degrees for a specific observation point (N33°293′486″ E126°163′985″) on *Jeju Island* in the Republic of Korea for an entire year. To train the RNN model represented in the next section, we employed the solar altitude, solar azimuth, and Earth-Sun distance as *learning features* to represent astronomical factors affecting solar irradiance.

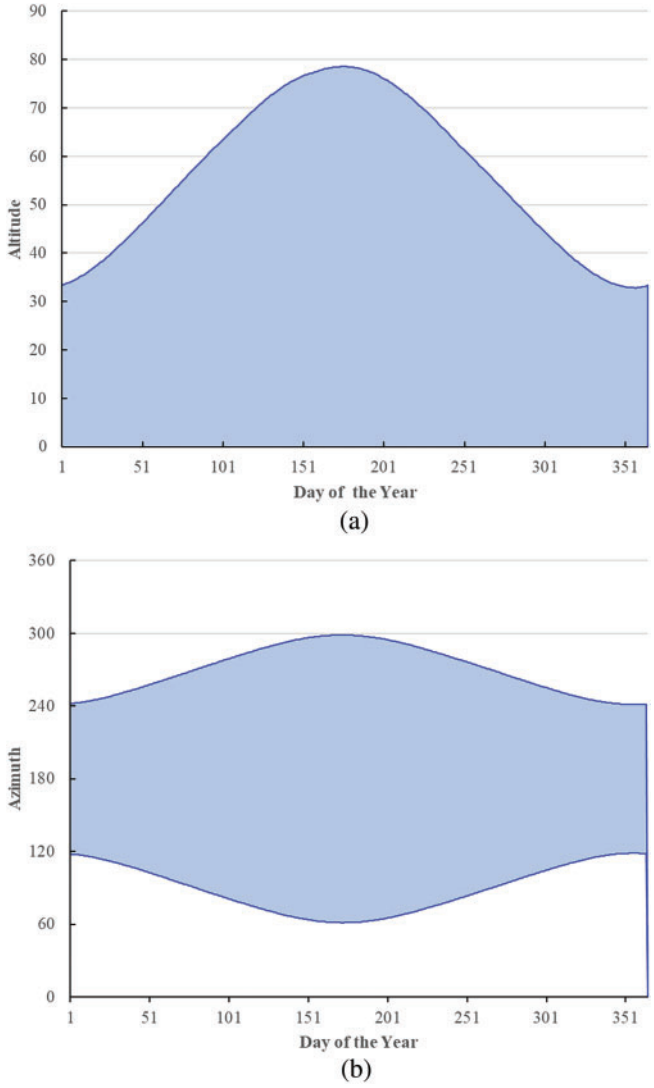

Figure 2: Solar altitude and azimuth variations during the year: (a) solar altitude variations and (b) solar azimuth variations

Atmospheric factors also play critical roles in influencing solar irradiance by modifying and attenuating sunlight as it passes through the Earth's atmosphere. These factors can influence the

intensity, spectral composition, and solar radiation distribution reaching the Earth's surface. Some important atmospheric factors affecting solar irradiance are *scattering*, *absorption*, *clouds*, *aerosols*, and *air masses*. These factors are summarized below:

- **Scattering:** Scattering occurs when particles and molecules in the atmosphere redirect solar irradiance in different directions. The two major types of scattering associated with solar irradiance are *Rayleigh scattering* and *Mie scattering*. Rayleigh scattering, which depends on the light wavelength, is more effective for shorter wavelengths, whereas Mie scattering is more pronounced for larger particles, such as dust and water droplets. In the air, aerosols primarily influence both types of scattering effects.
- **Absorption:** Atmospheric gases, such as *ozone* (O_3), *carbon dioxide* (CO_2), *nitrogen oxides* (NO_x), *water vapor* (H_2O), and *trace gases* (e.g., aerosols), absorb specific wavelengths of solar irradiance. This absorption reduces solar irradiance at that wavelength. The absorbed amount depends on the concentration and distribution of these gases in the atmosphere.
- **Clouds:** Clouds also significantly influence solar irradiance by reflecting, scattering, and absorbing solar radiation, changing the intensity and spectral distribution of solar irradiance on the Earth's surface. The extent, thickness, and type (e.g., *stratus*, *cumulus*, or *cirrus*) of clouds determine the magnitude of their effect on solar irradiance.
- **Aerosols:** Aerosols are tiny solid or liquid particles suspended in the air, which can come from natural sources (e.g., *dust* or *volcanic emissions*) or human activities (e.g., *industrial* or *vehicle emissions*). Aerosols can affect solar irradiance directly or indirectly by scattering and absorbing solar radiation. Direct scattering of sunlight by aerosols reduces the amount of solar radiation reaching the surface. In contrast, indirect effects involve aerosols acting as cloud condensation nuclei, altering cloud properties and influencing solar irradiance.
- **Air Mass:** Air mass measures the path length of sunlight through the Earth's atmosphere. As sunlight passes through the thicker atmosphere, scattering and absorption increase, reducing solar irradiance. The concept of air mass is quantified using the *air mass index* (AM), where a value of 1 represents direct sunlight (normal incidence), and a higher value indicates a longer path length and greater atmospheric attenuation. Air mass can be approximated as follows:

$$AM \approx \frac{1}{\cos z} \tag{1}$$

where z denotes the *solar zenith angle* [27].

Understanding and quantifying the effects of these atmospheric features are essential for accurate solar irradiance estimation and prediction. Advanced models and measurements integrating atmospheric properties and dynamics improve the accuracy of solar resource assessment, enhance the design and performance of solar energy systems, and enable the effective planning and integration of solar energy into energy grids.

To obtain actual measurements of atmospheric factors, we employed the public dataset of the *Korea Meteorological Administration* (KMA). The KMA provides a wealth of measurement data related to weather that can affect solar irradiance. The original dataset and its detailed description are available at the KMA website [28,29].

Considering all factors influencing solar irradiance, we applied some selected data for the training dataset as listed in Table 1. The dataset was acquired from an observation center at N33°17′37″, E126°9′46″, with an elevation of 71 m above sea level.

Table 1: Atmospheric features selected for solar irradiance prediction

Category	Meteorological data
Scattering	Relative humidity, dew point
Absorption	O_3 concentration, CO_2 concentration, NO_x concentration, N_2O concentration
Clouds	Visibility, cloud cover, wind speed, wind direction
Aerosols	Fine-dust concentration, cloud condensation nuclei
Air mass	Temperature, vapor pressure, sea-level pressure, atmosphere pressure
	16 features total

Fig. 3 presents a *normalized violin plot* representing features in Table 1, collected hourly from 2018 to 2021. The plot indicates that most measured values, except for the fine-dust concentration measurement, display well-distributed patterns. Despite efforts to resolve the spike in the value in this measurement, further investigation found that the recorded values matched an accurate reading of fine-dust concentrations in 2021.

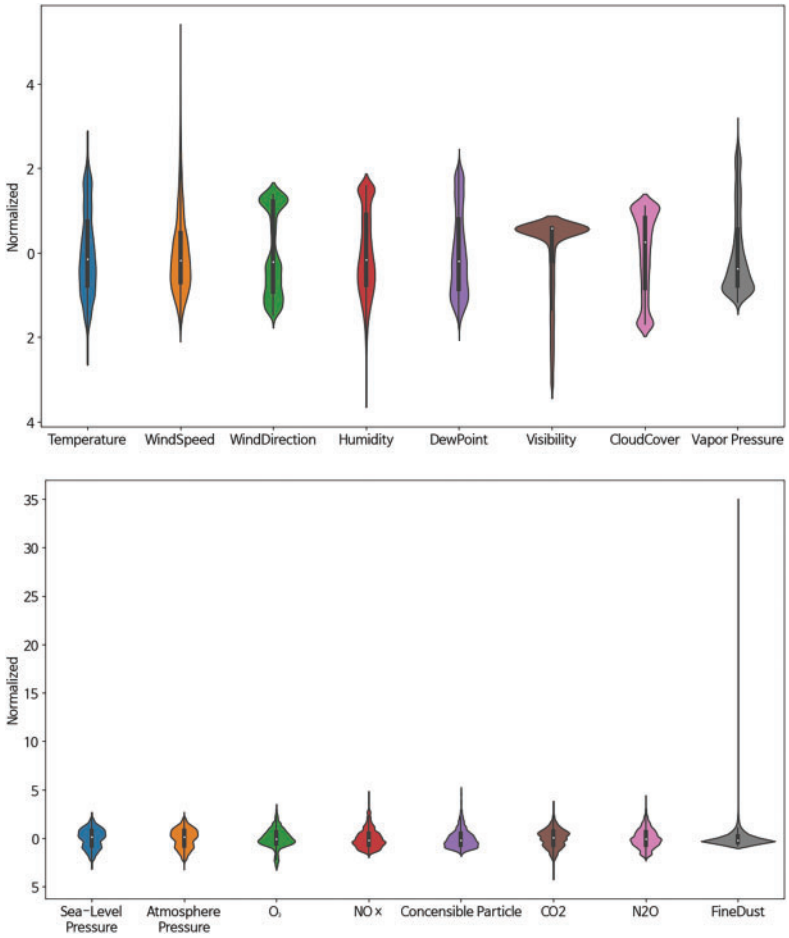

Figure 3: Normalized violin plots for meteorological features

3 Solar Irradiance Prediction with RNN

Accurate solar irradiance measurement at any location is desirable. However, solar irradiance measurements have only been made at designated locations, such as geodetic stations, and in particular, data accumulated over many years are available only at designated locations. This paper focused on estimating solar irradiance even in locations without accumulated data. Therefore, we present a method of predicting solar irradiance at a specific location through training with solar irradiance data using artificial intelligence deep learning techniques.

The KMA provides hourly solar irradiance measurements at designated observation locations. Fig. 4 presents an example set of daily solar irradiance measurements from 2018 to 2019. The presented method employs these datasets as training and prediction data for the machine learning models. Table 2 presents statistical information for the solar irradiance datasets.

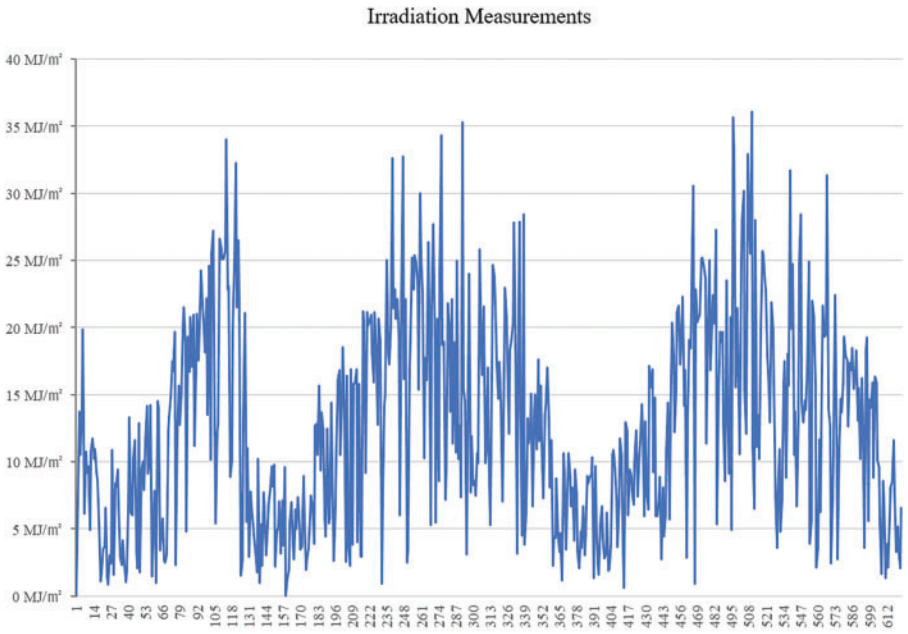

Figure 4: Solar irradiance measurements from 2018 to 2019, with the continuous day numbers on the horizontal axis, from Day 1 to late autumn 2019

Table 2: Statistics of solar irradiance data

Category	Value (MJ/m^2)
Mean	1.016514
Std Dev	0.962585
Min (or 0%)	0.000000
25%	0.170000
50%	0.700000
75%	1.730000
Max (or 100%)	3.500000

The RNNs are designed to process and analyze sequential data. Unlike traditional feed-forward neural networks presented in Fig. 5a, RNNs have connections that allow information to flow from input to output and in loops, creating a kind of memory, as illustrated in Fig. 5b. Therefore, RNNs are suitable for tasks involving sequential or time-dependent data, such as natural language processing, speech recognition, and time-series analysis [30,31].

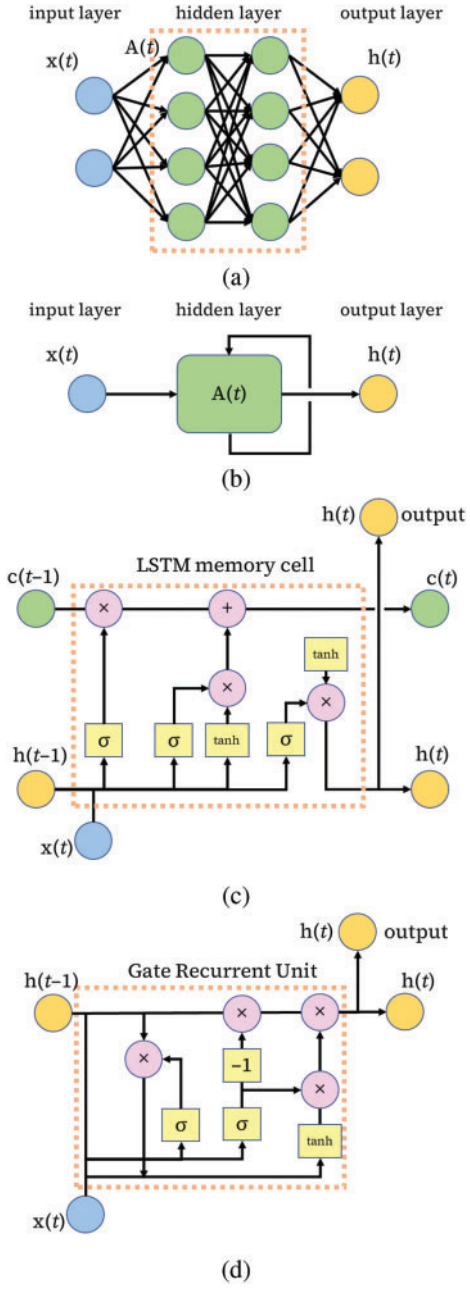

Figure 5: Diagrams of each recurrent neural network (RNN) method: (a) basic neural network, (b) RNN, (c) long short-term memory (LSTM), and (d) gated recurrent unit (GRU)

The RNN takes an input vector and a hidden state vector at each time step. The hidden state captures information from previous time steps, effectively allowing the network to retain information about observed sequences. This hidden state is updated at each time step, based on the current input and the previous hidden state, and becomes the input for the next time step. This circular structure allows the RNN to consider the context and dependencies in sequential data. One of the critical features of the RNN is the ability to handle sequences of variable lengths. The network can process sequences of various lengths by distributing the computation over the entire sequence, effectively creating a series of interconnected layers. This approach allows RNNs to capture long-term dependencies and extract meaningful patterns from sequences of any length [30,31].

Despite their potential, traditional RNNs can be limited in their ability to capture long-term dependencies due to the vanishing gradient problem. The LSTM and GRU variants have been developed to address this problem (Fig. 5c and d). These variations introduce additional mechanisms, such as gating devices, to retain or discard information selectively over time, improving the ability of the model to capture and propagate relevant information over longer sequences [32].

4 Solar Irradiance Prediction Results

This work performs *supervised learning* using RNN techniques comprising four layers in the network structure. Fig. 6 presents an abstract representation of the network layout applied in the experiment. Drop-out regularization with a ratio of 0.2 was incorporated into the network layer to avoid over-reliance on specific features and address the overfitting problem. Dense layers have also been employed to predict individual solar irradiance values. Each network layer can be modified to incorporate a specific RNN layer, including simple memoryless RNNs, LSTMs, and GRUs.

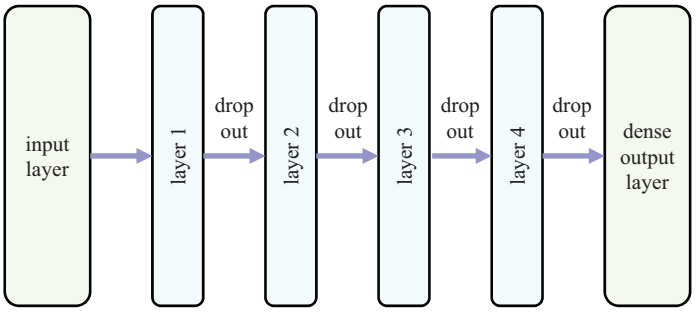

Figure 6: Network layout of the experiments

In the analysis of the experimental results, the error metrics of the *root mean squared error* (*RMSE*) and *mean absolute error* (*MAE*) were applied as follows:

$$RMSE = \sqrt{\sum_{i=1}^{n} \frac{(y_i - y_p)^2}{n}} \tag{2}$$

and

$$MAE = \frac{1}{n} \sum_{i=1}^{n} |y_i - y_p| \tag{3}$$

where y denotes the input and predicted values, and n represents the number of sampling points.

The network layout in the experiments was carefully designed to take full advantage of each RNN type. A critical criterion of layer design is to prove which combination of layers performs best for the presented extensive feature list of weather datasets in the feature selection section. The first layout consisted of four simple RNN layers. The second layout contained four LSTM layers, and the third layout contained four GRU layers. This study also explored two hybrid layouts. The fourth layout comprises two LSTM layers and two GRU layers in series, and the fifth layout consists of two LSTM layers between the GRU and RNN layers. This work investigated the performance and efficiency of various combinations of RNN layers for solar irradiance prediction using these configurations. The prediction results of the DNNs were compared to their performance with RNNs.

For each configuration, an *adaptive moment estimation* (ADAM) [33,34] with a learning ratio of 0.001, $\varepsilon = 10^{-8}$, $\beta_1 = 0.9$, and $\beta_2 = 0.999$ was applied for model fitting. For each neural network layer, the *arc tangent* function (tanh) was employed for activation, and the *sigmoid* function was applied for the recurrent step activation. The weight matrix for each neural network layer was initialized using the *Xavier* normal initializer [35] for every step, drawing the weight w from a normal distribution with a mean of zero and standard deviation as follows:

$$\sigma = \sqrt{\frac{2}{\text{inputs} + \text{outputs}}}$$

Figs. 7–9 display plots of the actual and projected values for solar irradiance. These figures reveal that the simple stack of RNN and GRU layers has difficulty accurately predicting zero irradiance values. In contrast, a stack of LSTM layers accurately predicted zero irradiance values compared with other network configurations. Combining several types of RNN layers did not significantly improve performance compared to LSTM layers alone. Additionally, RNN layer stacks tend to overpredict solar radiation values compared with other network configurations. The figure also reveals that RNNs work more effectively in forecasting solar irradiance than DNNs. These trends are reflected in detail in Table 3.

Table 3 presents the error metrics from the experiments. A conventional linear regression model is included as a reference in the first row of Table 3. The results reveal that the *linear regression* model has higher error metrics than other proposed methods, achieving an RMSE of 0.4647 and MAE of 0.5986. Although the other network layouts also display satisfactory results, the layout with four LSTM layers predicted solar irradiance best, achieving an RMSE of 0.2467 and MAE of 0.1203. Considering the equations for calculating the RMSE and MSE, we preferred MSE for the selection criteria because the RMSE may not be effective for lower error values of less than 1. Thus, we chose the configuration of four LSTM layers rather than the other network layout of two LSTM and two GRU layers with a lower RMSE value of 0.2185 but a higher MAE value of 0.1209. The following section applies a layout consisting of four LSTM layers as the solar irradiance prediction model.

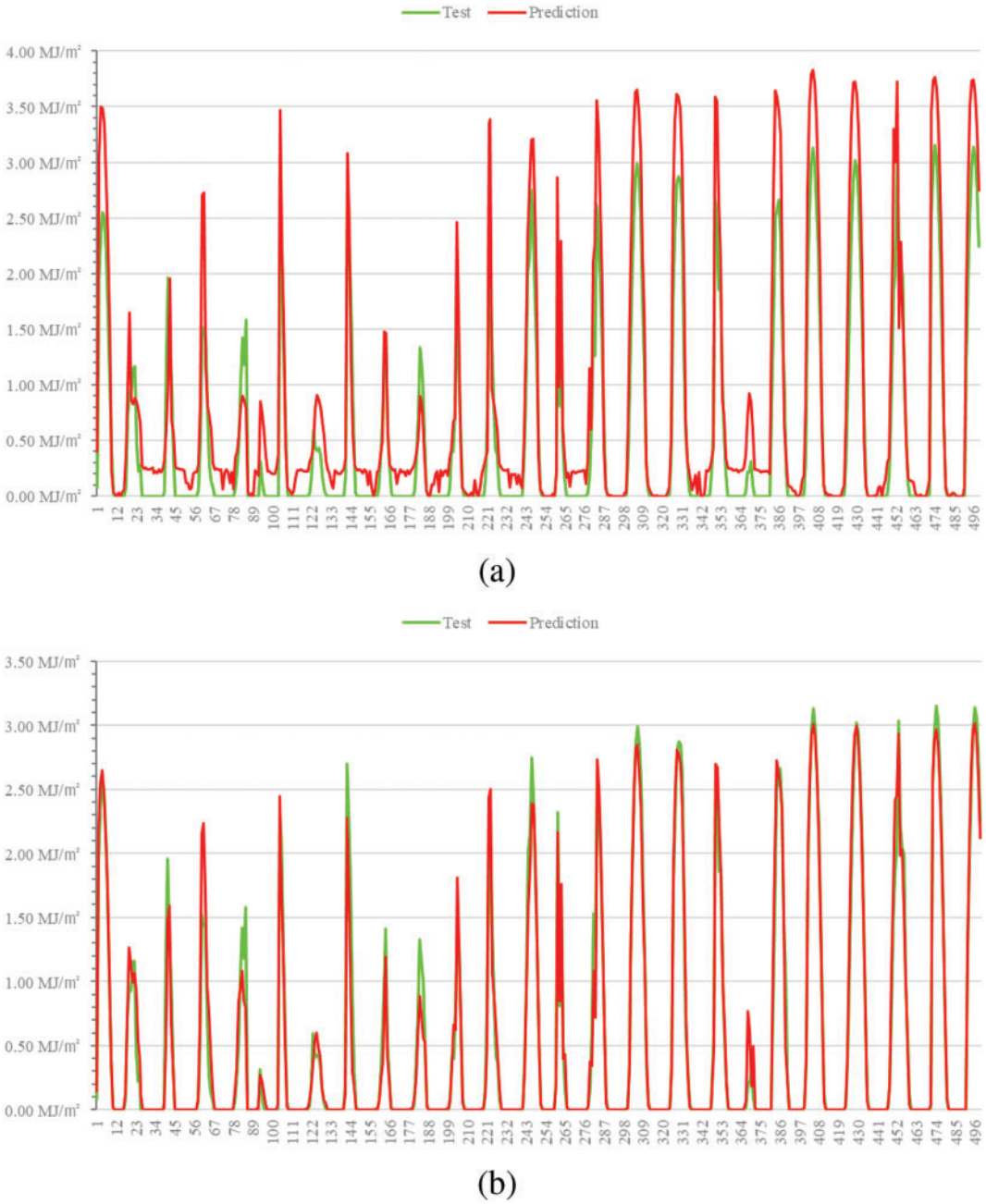

Figure 7: Actual and prediction value plots for solar irradiance, with day numbers on the horizontal axis using (a) 4 RNN layers and (b) 4 LSTM layers

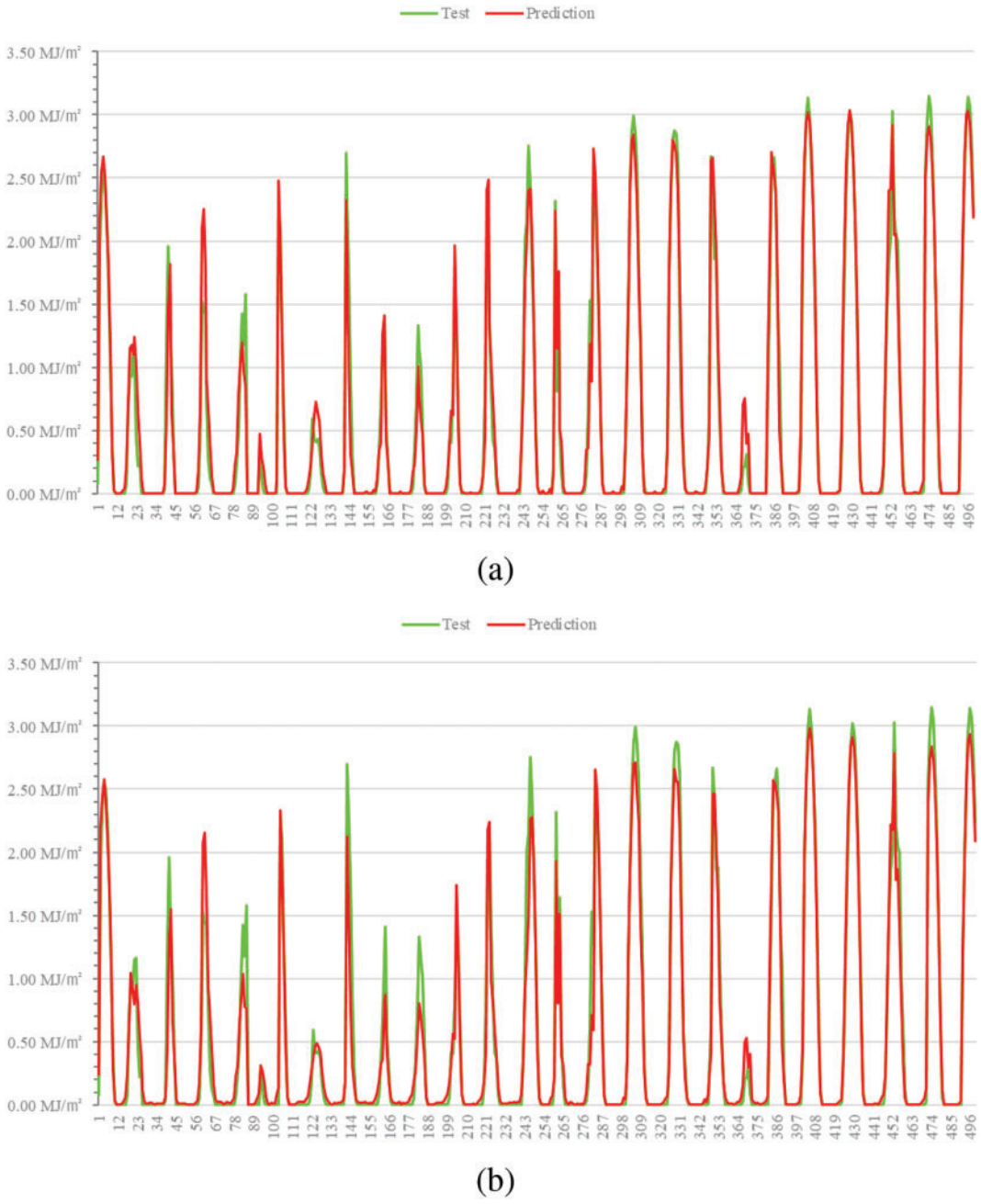

Figure 8: Actual and prediction value plots for solar irradiance, with day numbers on the horizontal axis, using (a) 4 GRU layers and (b) LSTM and GRU layers crosswise

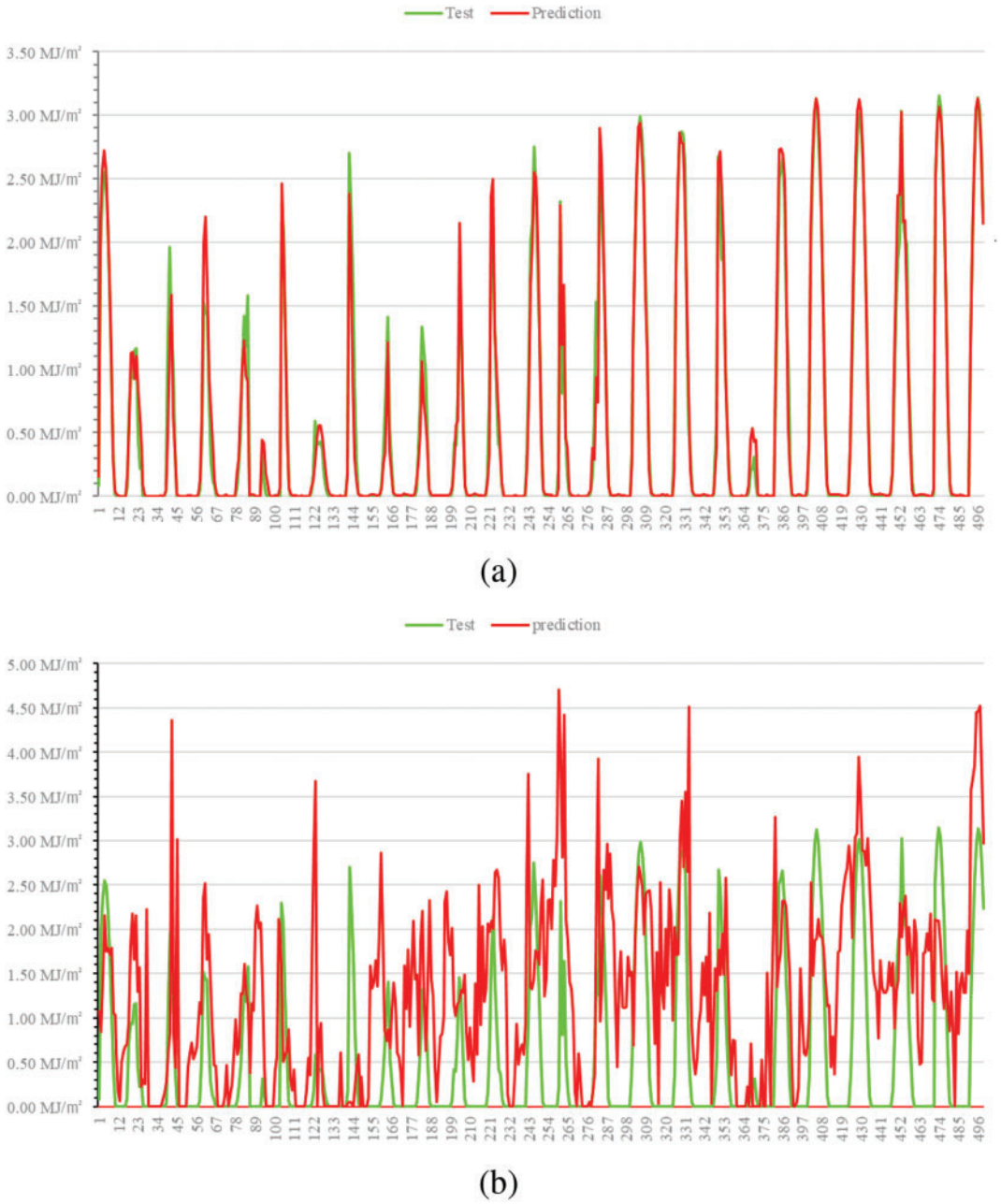

Figure 9: Actual and prediction value plots for solar irradiance, with day numbers on the horizontal axis, using (a) the GRU, LSTM, and RNN layers combined and (b) 4 DNN layers

Table 3: Solar irradiance prediction results for each method

Configuration	RMSE*	MAE†
Linear regression	0.4647	0.5986
4 RNN layers	0.4440	0.3144
4 LSTM layers	0.2467	0.1203
4 GRU layers	0.2532	0.1283
2 LSTM + 2 GRU layers	0.2185	0.1209
2 LSTM + 1 GRU + 1 RNN layers	0.2563	0.1270
4 DNN layers	2.4795	0.9932

Note: * root mean squared error † mean absolute error.

Several studies have focused on predicting hourly solar irradiance [36–38]. For example, one study [36] proposed solar irradiance prediction with data acquired from a ground station, and another [39] designed a solar irradiance prediction model using satellite images. Table 4 presents the best-performing annual RMSE values, converted to W/m^2, for the forecast models proposed in each of these papers, along with the RMSE from the current study. The results indicate that the proposed method outperforms the models presented in previous work [36,38], and [39]. However, the performance falls short of the results reported in Ref. [37], primarily due to geographical factors specific to the prediction area. Moreover, one study [38] represented predictions for a region near that for this study, and the final values indicate that the proposed method outperforms the previous methods [38].

Table 4: Results of the hourly solar irradiance prediction methods

Method	RMSE* (W/m^2)
Li et al. [36]	84.95
Kumari et al. [37]	58.08
Yeom et al. [38]	70.58
Ayet et al. [39]	98.00
Proposed method	68.53

Note: * root mean squared error.

5 Accumulated Shadow Map Generation

This paper proposes an innovative approach to solar irradiance prediction, integrating the surrounding environment based on computer graphics techniques. Solar radiance prediction using computer graphics employs 3D modeling and rendering techniques to simulate the solar radiance distribution in a virtual environment. Computer graphics techniques can realistically estimate solar irradiance patterns by considering numerous factors, such as the position of the Sun, terrain elevation, shading from buildings and vegetation, and atmospheric conditions.

The advantage of using computer graphics techniques for solar irradiance prediction is that the results can be visualized and analyzed in a realistic 3D environment. This approach helps design and optimize solar energy systems by better understanding how solar radiation interacts with the

surrounding objects and surfaces [40–42]. This method also employs computer graphics to evaluate the influence of architectural design, urban planning, and vegetation on solar irradiance to make informed decisions about renewable energy projects.

The presented method simulates shadows cast by the Sun by incorporating the Sun as a light source in the 3D graphics scenes using the solar azimuth and altitude values calculated in the previous section. The presented method fully applies the capabilities of modern graphics pipelines, specifically the *Open Graphics Library* (OpenGL) framework [43–45], and implements the shadow calculation algorithms as *OpenGL Shader Language* (GLSL) programs [46,47] to achieve this simulation. These programs can be efficiently executed on modern GPU architectures by concurrently generating accurate shadows in real time [48,49]. The generated shadows are cast at specific elevation levels to represent solar radiation patterns in the simulation environment. These shadows projected onto the ground surface are called *shadow maps*. The presented method typically employs shadow maps on the ground surface but can also use any elevation level surface to support different cases.

The shadow map provides only the shadow information at a specific time; hence, a method for analyzing the amount of sunlight over a period is required. To solve this problem, we propose a technique to *accumulate* shadow maps over time. The user specifies the duration of the solar irradiance simulation, which can span hours, days, weeks, months, or years. By accumulating shadow maps over the desired period, the proposed method can comprehensively understand solar irradiance patterns and changes over extended periods, allowing for more robust analyses and planning of solar energy systems.

The accumulation of shadow maps can be efficiently achieved using the *Compute Unified Device Architecture* (CUDA) [50–52], as follows:

$$M_{\text{acc}} = \frac{1}{n}\sum_{i=1}^{n} M_i \tag{4}$$

where M_{acc} denotes the final accumulated 2D image, and M_i represents the shadow map for the ith time point.

Fig. 10 presents the overall process of generating an *accumulated shadow map* and the sequential steps involved in the accumulation process. We implemented the accumulation algorithm in parallel with CUDA to provide a comprehensive representation of solar irradiance over a period. All these steps are performed in parallel with modern GPUs to achieve pseudo-real-time processing.

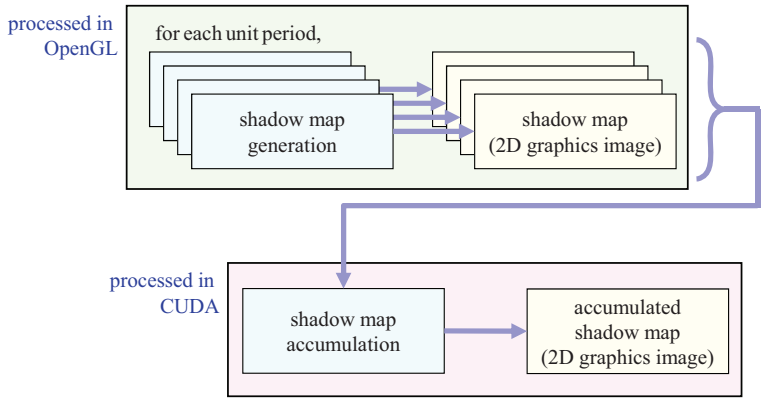

Figure 10: Generating accumulated shadow maps

6 Case Study with Surrounding Buildings

This paper estimates solar irradiance patterns for a specific location and period by training using the existing solar irradiance data via deep learning methods. Then, based on the OpenGL and CUDA libraries, we generated a shadow map by accumulating solar irradiance data over a specific period. Finally, this section presents a case study demonstrating that the proposed method works effectively.

Fig. 11 illustrates the 3D urban environment of the case study. In this environment, we estimate the ground-level solar irradiance, surrounded by buildings of various heights, for 2023. We generated an accumulated shadow map for the given configuration over the year (Fig. 12). Moreover, we identified several interest points, labeled P_1 to P_9, to measure the corresponding shadowing values. Table 5 lists these measurements. With an annual irradiance prediction of $V_{\text{ann}} = 4915.42$ MJ/m^2 from the prediction model, the proposed model can calculate the predicted solar irradiance values for the entire year by considering the accumulated shadow map and shadowing measurements at the interest points.

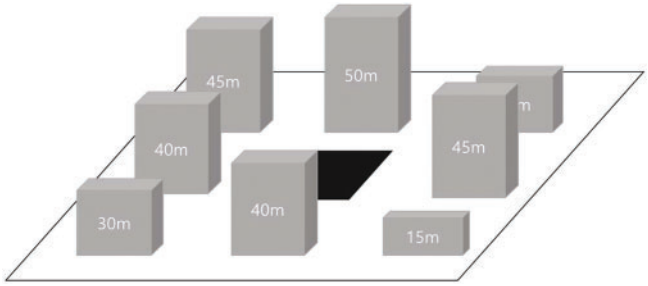

Figure 11: Three-dimensional configuration example for solar irradiance prediction

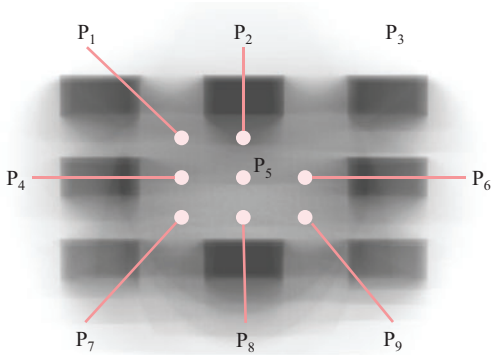

Figure 12: Accumulated shadow map for the three-dimensional configuration example

Table 5: Solar irradiance results for the three-dimensional configuration example

Points	Ratio (R)	Predicted irradiance ($R \cdot V_{\text{ann}}$)
P_1	0.5725	2814.078 MJ/m^2
P_2	0.4352	2139.191 MJ/m^2
P_3	0.6078	2987.592 MJ/m^2

(Continued)

Table 5 (continued)

Points	Ratio (R)	Predicted irradiance ($R \cdot V_{\text{ann}}$)
P_4	0.5607	2756.076 MJ/m^2
P_5	0.6000	2949.252 MJ/m^2
P_6	0.5529	2717.736 MJ/m^2
P_7	0.6352	3122.275 MJ/m^2
P_8	0.6667	3277.111 MJ/m^2
P_9	0.6392	3141.936 MJ/m^2

Solar irradiance simulation using 3D graphics is not a widely researched area. Thus, we could not locate a reliable reference model. Instead, we applied a web-based application called *ShadeMap* [53], a model-based prediction model. *ShadeMap* is a closed-source, free-to-use, web-based application that can simulate solar irradiance with given scenarios.

Table 6 compares the results from the proposed model and *ShadeMap*. Both methods apply different models; hence, we cannot determine which is better. However, we can determine that both models display similar simulation patterns. For example, Point P_2 exhibits the lowest value, and Point P_8 has the highest value for both models. The correctness or accuracy of the simulation should be further explored.

Table 6: Comparison of the results of solar irradiance using *ShadeMap*

Points	Predicted irradiance	emphShadeMap results
P_1	2814.078 MJ/m^2	3132 MJ/m^2
P_2	2139.191 MJ/m^2	2362 MJ/m^2
P_3	2987.592 MJ/m^2	3493 MJ/m^2
P_4	2756.076 MJ/m^2	3008 MJ/m^2
P_5	2949.252 MJ/m^2	3298 MJ/m^2
P_6	2717.736 MJ/m^2	3094 MJ/m^2
P_7	3122.275 MJ/m^2	3331 MJ/m^2
P_8	3277.111 MJ/m^2	3954 MJ/m^2
P_9	3141.936 MJ/m^2	3451 MJ/m^2

7 Conclusion

This paper presented a set of solar irradiance models using RNNs with configured layers. Among them, the layout consisting of four LSTM layers performed the best. This layout achieved reasonable error bounds, with an RMSE of 0.2467 and an MAE of 0.1203. Based on this prediction model, this paper proposed a computer graphics-based solar irradiance prediction model incorporating simulations of the surrounding environment. This simulation generates shadow maps for a specific time, accumulating them into a single shadow map. The proposed method lets the user obtain the corresponding solar irradiance prediction values. We presented a case study with surrounding

buildings and analyzed the solar irradiance over the entire year to demonstrate the feasibility of the proposed method.

We plan to further improve the solar irradiance prediction model's accuracy and efficiency by incorporating additional elements. Such elements include varying the training and testing dataset features by collecting more significant weather data related to solar irradiance, modifying the layers of the neural networks to the state-of-the-art RNN layer, which is the *fuzzy-embedded RNN* [54], or *deblurring* [55]. We also plan to improve the user interfaces for smoother interactions.

Acknowledgement: The authors would like to express our sincere appreciation to the Editors and Reviewers for their valuable insights and continuous encouragement.

Funding Statement: This work was supported by the MSIT (Ministry of Science and ICT), Republic of Korea, under the ITRC (Information Technology Research Center) support program (IITP-2024-RS-2024-00437756) supervised by the IITP (Institute for Information & Communications Technology Planning & Evaluation). This work was also supported by the BK21 FOUR project (AI-driven Convergence Software Education Research Program) funded by the Ministry of Education, School of Computer Science and Engineering, Kyungpook National University, Republic of Korea (4120240214871).

Author Contributions: The authors confirm contribution to the paper as follows: study conception and design: Woosuk Shin, Nakhoon Baek; data collection: Woosuk Shin; analysis and interpretation of results: Woosuk Shin, Nakhoon Baek; draft manuscript preparation: Woosuk Shin, Nakhoon Baek. All authors reviewed the results and approved the final version of the manuscript.

Availability of Data and Materials: The data that support the findings of this study are available from the corresponding author upon reasonable request.

Ethics Approval: Not applicable.

Conflicts of Interest: The authors declare no conflicts of interest to report regarding the present study.

References

1. Baredar P, Shukla A. Simulation and performance analysis of 110 kWp grid-connected photovoltaic system for residential building in India: a comparative analysis of various PV technology. Energy Rep. 2016;2(5):82–8. doi:10.1016/j.egyr.2016.04.001.
2. Saber EM, Lee SE, Manthapuri S, Yi W, Deb C. PV (photovoltaics) performance evaluation and simulation-based energy yield prediction for tropical buildings. Energy. 2014;71:588–95. doi:10.1016/j.energy.2014.04.115.
3. Diagne M, David M, Lauret P, Boland J, Schmutz N. Review of solar irradiance forecasting methods and a proposition for small-scale insular grids. Renew Sustain Energ Rev. 2013;27:65–76. doi:10.1016/j.rser.2013.06.042.
4. Li J, Ward JK, Tong J, Collins L, Platt G. Machine learning for solar irradiance forecasting of photovoltaic system. Renew Energy. 2016;90(7):542–53. doi:10.1016/j.renene.2015.12.069.
5. Obiora CN, Ali A, Hasan AN. Forecasting hourly solar irradiance using long short-term memory (LSTM) network. In: 2020 11th International Renewable Energy Congress (IREC); 2020; NY, USA: IEEE. p. 1–6. doi:10.1109/IREC48820.2020.9310449.

6. Rhouma A, Said Y. Solar energy forecasting based on complex valued auto-encoder and recurrent neural network. Int J Adv Comput Sci Appl. 2023;14(4). doi:10.14569/IJACSA.2023.0140443.
7. Alomari MH, Younis O, Hayajneh SMA. A predictive model for solar photovoltaic power using the Levenberg-Marquardt and Bayesian regularization algorithms and real-time weather data. Int J Adv Comput Sci Appl. 2018;9(1). doi:10.14569/IJACSA.2018.090148.
8. Kumari P, Toshniwal D. Deep learning models for solar irradiance forecasting: a comprehensive review. J Clean Prod. 2021;318(3):128566. doi:10.1016/j.jclepro.2021.128566.
9. Alzahrani A, Shamsi P, Dagli C, Ferdowsi M. Solar irradiance forecasting using deep neural networks. Procedia Comput Sci. 2017;114(7):304–13. doi:10.1016/j.procs.2017.09.045.
10. Yu Y, Cao J, Zhu J. An LSTM short-term solar irradiance forecasting under complicated weather conditions. IEEE Access. 2019;7:145 651–66. doi:10.1109/ACCESS.2019.2946057.
11. Husein M, Chung I-Y. Day-ahead solar irradiance forecasting for microgrids using a long short-term memory recurrent neural network: a deep learning approach. Energies. 2019;12(10):1856. doi:10.3390/en12101856.
12. Jaihuni M, Basak JK, Khan F, Okyere FG, Sihalath T, Bhujel A, et al. A novel recurrent neural network approach in forecasting short term solar irradiance. ISA Trans. 2022;121:63–74. doi:10.1016/j.isatra.2021.03.043.
13. Bejani MM, Ghatee M. A systematic review on overfitting control in shallow and deep neural networks. Artif Intell Rev. 2021;54(8):6391–438. doi:10.1007/s10462-021-09975-1.
14. Salman S, Liu X. Overfitting mechanism and avoidance in deep neural networks. 2019. doi:10.48550/arXiv.1901.06566.
15. Cogswell M, Ahmed F, Girshick RB, Zitnick L, Batra D. Reducing overfitting in deep networks by decorrelating representations. In: 4th International Conference on Learning Representations, ICLR 2016; 2016. doi:10.48550/arXiv.1511.06068.
16. Sze V, Chen Y-H, Yang T-J, Emer JS. Efficient processing of deep neural networks: a tutorial and survey. Proc IEEE. 2017;105(12):2295–329. doi:10.1109/JPROC.2017.2761740.
17. Samek W, Montavon G, Lapuschkin S, Anders CJ, uller K-RM. Explaining deep neural networks and beyond: a review of methods and applications. Proc IEEE. 2021;109(3):247–78. doi:10.1109/JPROC.2021.3060483.
18. Hochreiter S. The vanishing gradient problem during learning recurrent neural nets and problem solutions. Int J Uncert Fuzzin Knowl-Based Syst. 1998;6(2):107–16. doi:10.1142/S0218488598000094.
19. Bamisile O, Cai D, Oluwasanmi A, Ejiyi C, Ukwuoma CC, Ojo O, et al. Comprehensive assessment, review, and comparison of AI models for solar irradiance prediction based on different time/estimation intervals. Sci Rep. 2022;12(1):9644. doi:10.1038/s41598-022-13652-w.
20. Kumar DS, Yagli GM, Kashyap M, Srinivasan D. Solar irradiance resource and forecasting: a comprehensive review. IET Renew Power Gener. 2020;14(10):1641–56. doi:10.1049/iet-rpg.2019.1227.
21. Aicardi D, Musé P, Alonso-Suárez R. A comparison of satellite cloud motion vectors techniques to forecast intra-day hourly solar global horizontal irradiation. Sol Energy. 2022;233(1):46–60. doi:10.1016/j.solener.2021.12.066.
22. Coiffier J. Fundamentals of numerical weather prediction. UK: Cambridge University Press; 2011.
23. Landat Missions. Earth-sun distance in astronomical units for days of the year. USGS, VA, USA: United States Geological Survey; 2019.
24. Grena R. An algorithm for the computation of the solar position. Sol Energy. 2008;82(5):462–70. doi:10.1016/j.solener.2007.10.001.
25. Rizal Y, Wibowo SH, Feriyadi. Application of solar position algorithm for sun-tracking system. Energy Proc. 2013;32:160–5. doi:10.1016/j.egypro.2013.05.021.

26. Reda I, Andreas A. Solar position algorithm for solar radiation applications. Sol Energy. 2004;76(5):577–89. doi:10.1016/j.solener.2003.12.003.
27. Gallery W, Kneizys F, Clough S. Air mass computer program for atmospheric transmittance/radiance calculation: FfSCATM. NM, USA: Air Force Geophysics Lab; 1983.
28. Korea Meteorological Administration. Automated synoptic observing system (ASOS) data; 2024 [cited 2024 Nov 10]. [Online]. Available from: https://data.kma.go.kr/data/grnd/selectAsosRltmList.do?pgmNo=36.
29. Korea Meteorological Administration. Manual for ground surveillance; 2022 [cited 2024 Nov 10]. Available from: https://data.kma.go.kr/resources/images/publication/%EC%A7%80%EC%83%81%EA%B8%B0%EC%83%81%EA%B4%80%EC%B8%A1%EC%A7%80%EC%B9%A8(2022.12.).pdf.
30. Jain LC, Medsker LR. Recurrent neural networks: design and applications. FL, USA: CRC Press, Inc; 1999.
31. Flores A, Tito H, Centty D. Recurrent neural networks for meteorological time series imputation. Int'l J Adv Comput Sci Appl. 2020;11(3):1. doi:10.14569/IJACSA.2020.0110360.
32. Salehinejad H, Baarbe J, Sankar S, Barfett J, Colak E, Valaee S. Recent advances in recurrent neural networks. 2018. doi:10.48550/arxiv.1801.01078.
33. Kingma DP, Ba J. Adam: a method for stochastic optimization. In: 3rd International Conference on Learning Representations (ICLR 2015); 2015. doi:10.48550/arXiv.1412.6980.
34. Kingma DP, Ba J. Adam: a method for stochastic optimization. 2017. doi:10.48550/arxiv.1412.6980.
35. Glorot X, Bengio Y. Understanding the difficulty of training deep feedforward neural networks. In: Proceedings of the Thirteenth International Conference on Artificial Intelligence and Statistics; 2010. Vol. 9, p. 249–56.
36. Li C, Zhang Y, Zhao G, Ren Y. Hourly solar irradiance prediction using deep BiLSTM network. Earth Sci Inform. 2020;14(1):299–309. doi:10.1007/s12145-020-00511-3.
37. Kumari P, Toshniwal D. Extreme gradient boosting and deep neural network based ensemble learning approach to forecast hourly solar irradiance. J Clean Product. 2021;279(8):123285. doi:10.1016/j.jclepro.2020.123285.
38. Yeom J-M, Deo R, Adamowski J, Park S, Lee CS. Spatial mapping of short-term solar radiation prediction incorporating geostationary satellite images coupled with deep convolutional LSTM networks for South Korea. Environ Res Lett. 2020;15(9):094025. doi:10.1088/1748-9326/ab9467.
39. Ayet A, Tandeo P. Nowcasting solar irradiance using an analog method and geostationary satellite images. Sol Energy. 2018;164(4):301–15. doi:10.1016/j.solener.2018.02.068.
40. Liang J, Gong J, Xie X, Sun J. Solar3D: an open-source tool for estimating solar radiation in urban environments. ISPRS Int J Geo-Inform. 2020;9(9):524. doi:10.3390/ijgi9090524.
41. Machete R, Falcão AP, Gomes MG, Moret Rodrigues A. The use of 3D GIS to analyse the influence of urban context on buildings' solar energy potential. Energy Build. 2018;177(14):290–302. doi:10.1016/j.enbuild.2018.07.064.
42. Chan Y-C, Tzempelikos A. A hybrid ray-tracing and radiosity method for calculating radiation transport and illuminance distribution in spaces with venetian blinds. Sol Energy. 2012;86(11):3109–24. doi:10.1016/j.solener.2012.07.021.
43. Segal M, Akeley K. The OpenGL graphics system: a specification, version 4.6 (Core Profile). OR, USA: Khronos Group; 2022.
44. Segal M, Akeley K. The OpenGL graphics system: a specification, version 4.6 (Compatibility Profile). OR, USA: Khronos Group; 2022.
45. Kim M, Baek N. A 3D graphics rendering pipeline implementation based on the OpenCL massively parallel processing. J Supercomput. 2021;77(7):7351–67. doi:10.1007/s11227-020-03581-8.
46. Kessenich J, Baldwin D, Rost R. The OpenGL shading language, version 4.60.7. OR, USA: Khronos Group; 2019.

47. Wolff D. OpenGL 4 shading language cookbook: build high-quality, real-time 3D graphics with OpenGL 4.6, GLSL 4.6 and C++17. 3rd ed. UK: Packt Publishing; 2018.
48. Baek N, Kim KJ. Design and implementation of OpenGL SC 2.0 rendering pipeline. Cluster Comput. 2019;22(1):931–6. doi:10.1007/s10586-017-1111-1.
49. Baek N. An emulation scheme for openGL SC 2.0 over openGL. J Supercomput. 2020;76(10):7951–60. doi:10.1007/S11227-018-2399-1.
50. NVIDIA. CUDA toolkit documentation, version 12.6. CA, USA: NVIDIA; 2024.
51. Kirk D. NVIDIA CUDA software and GPU parallel computing architecture. In: Proceedings of the 6th International Symposium on Memory Management (ISMM '07); 2007. p. 103–4. doi:10.1145/1296907.1296909
52. Sanders J, Kandrot E. CUDA by example: an introduction to general-purpose GPU programming. MA, USA: Addison-Wesley Professional; 2017.
53. ShadeMap. shademap.app. [cited 2024 Nov 10]. Available from: https://shademap.app/.
54. Tan JCM, Cao Q, Quek C. FE-RNN: a fuzzy embedded recurrent neural network for improving interpretability of underlying neural network. Inf Sci. 2024;663(C):120276. doi:10.1016/j.ins.2024.120276.
55. Ma Z, Zhang H, Liu J. DB-RNN: an RNN for precipitation nowcasting deblurring. IEEE J Select Top Appl Earth Observat Remote Sens. 2024;17:5026–41. doi:10.1109/JSTARS.2024.3365612.